Peer-reviewed version available at Molecules 2018, 23, 1320; doi:10.3390/molecules23061320

Article

Computational insight into the effect of natural compounds on the destabilization of preformed amyloid-β(1-40) fibrils

Francesco Tavanti*, Alfonso Pedone and Maria Cristina Menziani*

Department of Chemical and Geological Sciences, University of Modena and Reggio Emilia, Via G. Campi, 103 – Modena, Italy.

* Correspondence: mariacristina.menziani@unimore.it, francesco.tavanti@unimore.it

Abstract: One of the principal hallmarks of Alzheimer's disease (AD) is related to the aggregation of amyloid-β fibrils in an insoluble form in the brain, also known as amyloidosis. Therefore, a prominent therapeutic strategy against AD consists either in blocking the amyloid aggregation and/or destroying the already formed aggregates. Natural products have shown significant therapeutic potential as amyloid inhibitors from *in vitro* studies as well as *in vivo* animal tests. In this study, the interaction of five natural biophenols (curcumin, dopamine, (-)-Epigallocatechin-3-gallate, Quercetin, and Rosmarinic acid) with the amyloid-β(1-40) fibrils has been studied through computational simulations. The results allowed the identification and characterization of the different binding modalities of each compounds and their consequences on fibril dynamics and aggregation. It emerges that the lateral aggregation of the fibrils is strongly influenced by the intercalation of the ligands, which modulate the double-layered structure stability.

Keywords: Molecular dynamics simulation; biophenols; natural compounds; amyloid fibrils; Alzheimer's disease; ligand-protofiber interactions.

1. Introduction

The pathological hallmark of AD is the extracellular accumulation of insoluble proteinaceous deposits called amyloid fibrils[1] that induce cytotoxicity. The formation of mature amyloid fibrils (Aβ) proceeds through a nucleation dependent process, where monomers and oligomers aggregate together forming β-sheets rich protein structures. The most common fibrils are Aβ(1-40) and Aβ(1-42) that are composed by 40 and 42 amino acids, respectively, and are characterized by β-strand units aligned perpendicular to the main fibril axis[2]. Destabilization and clearance of amyloid aggregates by small molecules is one of the promising approaches towards the development of AD therapies[4].

In the last years, epidemiological studies on the effects of the diet against AD and dementia suggested that the high intake of flavonoids and polyphenols found in fruits and vegetables reduces the risk of AD and cognitive impairments, and several natural molecules have been identified to promote cognitive health and to interfere with the amyloidogenic activity in AD[11].

A detailed knowledge of how these molecules interact with Aβ fibrils is a prerequisite for the design of new efficient drugs. Unfortunately, despite intensive researches, the experimental characterization of full-length Aβ oligomers/inhibitor complexes at a high level of resolution remains a great challenge.

Atomistic computer simulations are well suited to provide molecular-level details of amyloid oligomer and fibril interactions with ligands, helping in the future development and characterization of druggable modalities[12]. Basically four aspects of the flavonoids-amyloid interaction have been studied by computational methods: 1) the effect of ligands on the conformational transitions of Aβ monomers from initial random coil or α-helix into β-sheet structures[13,14] and ligand-mediated conformational change on Aβ dimer[15] by means of Replica Exchange Molecular Dynamics (REMD) simulations; 2) the effect of ligands on the aggregation of Aβ(17–36) using Coarse-Grained

Simulations[16]; 3) effect of ligands on the conformation and stability of amyloid-beta mutants[17] by Molecular Dynamics (MD) simulations; 4) preferential binding sites of ligands and their effect on amyloid structure-dynamics[18] on Aβ fragments and full-length single Aβ protofilament[19–25] by means of Docking experiments, MD simulations and Free Energy calculations.

Although recently a few studies devoted their attention to the interaction of ligands (mainly markers for amyloid detection ref. [26–28]) with multiple Aβ protofilaments, to the best of our knowledge this aspect has not been investigated thoroughly for natural polyphenol ligands, except for curcumin[19].

In this study, the binding modalities of five natural biophenols (curcumin, dopamine, (-)-Epigallocatechin-3-gallate, Quercetin, and Rosmarinic acid) with single Aβ(1-40) protofilament and double-layer oligomers aggregates will be studied through atomistic computational simulations in order to explore structural changes in aggregate pathways upon binding.

First, putative binding sites on the Aβ(1-40) protofibril will be explored by replica exchange molecular dynamics (REMD) simulations. Then, binding free energies (ΔG_{bind}) will be computed on the complexes to determine the thermodynamically favourite binding modalities. Finally, the structural effects caused by the binding of polyphenols to two double-layer protofilament polymorphs will be assessed. To this goal the determination of the stability of the sheet-to-sheet associations of the double-layered organizations with and without the polyphenols will be computed by means of the Potential of Mean Force (PMF) methodology.

2. Methods

2.1 Molecular Dynamics Simulations

Molecular dynamics simulations were performed with GROMOS 54a7 force field[29]. The structural model of amyloid fibrils was retrieved from the PDB[30] (PDB ID: 2LMN[31]). From this structure, an Aβ monomer was isolated and the missing N-terminal peptide region of Aβ(1-40) monomer (^{1}DAEFRHDS^{8}) was built using the Molefacture plugin in the VMD package[32] as random coils as predicted by both the Jpred web server[33] and by the Modeller package[34] for protein secondary structure assignments. Standard protonation states corresponding to pH 7 were assigned to ionisable residues. The Aβ(1-40) protofibril was composed by repeating 10 monomeric units along its principal axis obtaining a continuous structure 5nm long.

The force field assigned to each ligand in their standard protonation states at pH 7 was built in the GROMACS format[35] by using the Automated Topology Builder[36,37] web server.

The simulation box (7.5x9.7x8.0xnm) contains one Aβ(1-40) protofibril composed by repeating 10 monomeric units, one ligand placed in a random position with respect to the fibril, and about 30000 simple point charge water molecules[38]. Counter ions (Na^+ and Cl^-) were added at random locations to neutralize the systems, with ion concentration of 150 mM, close to the physiological value.

All the simulations were carried out at physiological temperature (310K) and pressure of 1 bar. The systems were first equilibrated for 2 ns in the NVT ensemble, then 10n runs were carried out in the NPT ensemble. The temperature was controlled using a velocity-rescaling thermostat with a coupling time of 0.1ps. During equilibration the Berendsen barostat was used to control the pressure, while during the production run the Parrinello-Rhaman barostat was used with coupling time of 2ps and an isothermal compressibility of 4.5×10^{-5} bar^{-1} and the timestep used was 2.0fs.The particle-mesh Ewald algorithm was used to calculate long-range electrostatics[39],[40] with a fourth-order cubic interpolation, a grid spacing of 0.16nm, and a real-space cutoff of 1nm. Both Van Der Waals and neighbour list cutoffs describing short-range interactions were set to 1.0 nm. A production run of 50 ns was used to identify the ligand binding sites (paragraph 2.2), whereas trajectories of 100 ns were necessary for the computation of the stability of the different protofibrils polymorphs (paragraph 2.4). Data analysis were performed using the GROMACS-5.0.4 package[41].

2.2 Ligand binding sites

Temperature Replica Exchange MD (REMD) simulations were used to define the most probable interacting sites of each compound with the Aβ(1-40) protofibrils. The temperatures used for replicas were obtained by the work of Patriksson and van der Spoel[42] and are reported below: 300.00, 301.16, 302.32, 303.49, 304.66, 305.83, 307.01, 308.19, 309.38, 310.57, 311.76, 312.96, 314.16, 315.37, 316.57, 317.78, 319.00, 320.22, 321.44, 322.66, 323.89, 325.12, 326.36, 327.60, 328.85, 330.09, 331.34, 332.60, 333.86, 335.12, 336.39, 337.66, 338.93, 340.21.

An acceptance ratio of 20% was chosen as previously suggested by Ngo et al.[43]. Each REMD simulation replica was equilibrated with an NVT and an NPT ensemble with the same parameters as for MD simulations. Then a 50ns run (i.e. the production run) was performed for each replica, exchanges between neighbouring replicas were checked every 500 steps corresponding to 1ps[43]. The 50ns simulations were used for data analysis.

2.3 Ligand binding energy

The Molecular Mechanics-Poisson-Boltzmann surface area (MM_PBSA) method [44] was used to calculate the binding energy of each ligand to the protofibril. This method is based on the single-trajectory approach. Thus, 100 snapshots collected consecutivelly over the course of the 50ns simulations, once the ligand reached a stable binding (i.e. rmsd of its center of mass < 5 Å, Figure S1) were used. The binding free energy ($\Delta G_{binding}$) is described as the free energy difference between the complex, $G_{complex}$, and the summation of the free energy of protein, $G_{protein}$, and ligand, G_{ligand}:

$$\Delta G_{binding} = G_{complex} - \left(G_{protein} + G_{ligand}\right) \quad (1)$$

The free energy of each molecule is given by

$$G = E_{MM} + G_{solvation} - T\Delta S \quad (2)$$

Where T and S represent the temperature and entropy, respectively, and the mechanical energy, E_{MM}, of the solute in the gas phase is given by the summation of bond, angles, dihedrals, Van der Waals and electrostatic terms:

$$E_{MM} = E_{bond} + E_{angle} + E_{digedral} + E_{electr} + E_{VdW} \quad (3)$$

The solvation energy, $G_{solvation}$, is calculated as follows:

$$G_{solvation} = G_{surf} + G_{PB} \quad (4)$$

Where the non-polar solvation term, G_{surf}, is approximated on the solvent-accessible-surface area (SASA) derived from the Shrake-Rupley numerical method[45]

$$G_{surf} = \gamma SASA + \beta \quad (5)$$

with γ=0.0072kcal/mol Å^2 and β=0[46].

The term comprising the electrostatic potential between the solute and the solvent, G_{PB}, is calculated using the continuum solvent approximation[47] by the APBS package[48].

The entropy term, $T\Delta S$, is computed using the Quasi-harmonic formula[49].

2.4 Aβ(1-40) oligomer double-layered structures

Two possible double-layered structures were build by stacking the β-sheets of each monomer onto each other in an antiparallel fashion[50,51], as shown in **Figure 1**. The C-terminal–C-terminal and N-terminal–N-terminal interfaces were, thus, obtained. The inter-sheet distance was computed

as the distance between the centres of mass of the two β-sheets that are in contact. The amino acids that were considered for the calculations of the centre of mass are H13, H14, Q15, K16, L17, V18, F19, F20, A21, E22 for the N-terminal–N-terminal interface (β-1 β-sheets) (**Figure 1a**) and A30, I31, I32, G33, L34, M35, V36, G37, G38, V39 for the C-terminal–C-terminal interface (β-2 β-sheets) (**Figure 1b**).

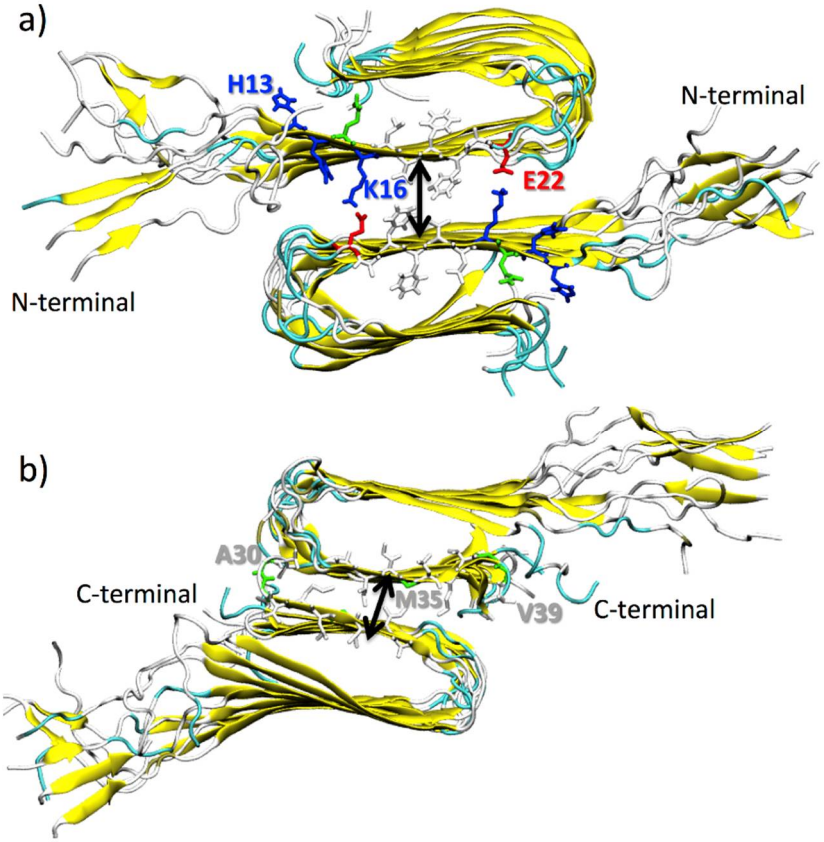

Figure 1. Cartoon representation of double-layered structures of Aβ(1-40) oligomers facing through their β-1, in a), and β-2 β-sheets, in b). Fibrils are coloured accordingly to their secondary structures. Amino acids at the interface are explicitly represented (colour code: blue for positive charged, red for negatively charged, and white for hydrophobic amino acid residues). Black arrows roughly represent the inter-sheet distance.

In order to evaluate the influence of the ligands on the stability of the different protofibrils polymorphs the Potential of Mean Force (PMF) method implemented in the GROMACS program was used[52,53].

The backbone of protofibril(1) was restrained in its starting position, while a force increasing with time, was assigned to the centre of mass of protofibril(2). Three directions were taken into account, as shown in **Figure 2**: the *x-axis* (i.e. outward), the *y-axis* (i.e. lateral) and the *z-axis* (i.e. vertical). For each ligand and for both protofibril contact modes (β-1 and β-2 β-sheets), three runs were performed using as starting configurations the ones at 90, 95 and 100 ns, ensuring good sampling. The starting force used at the beginning of the simulation was 1000 kJ/mol nm^2 and the rate at which the application point of the force moves was 0.01 nm/ps.

Peer-reviewed version available at *Molecules* **2018**, *23*, 1320; doi:10.3390/molecules23061320

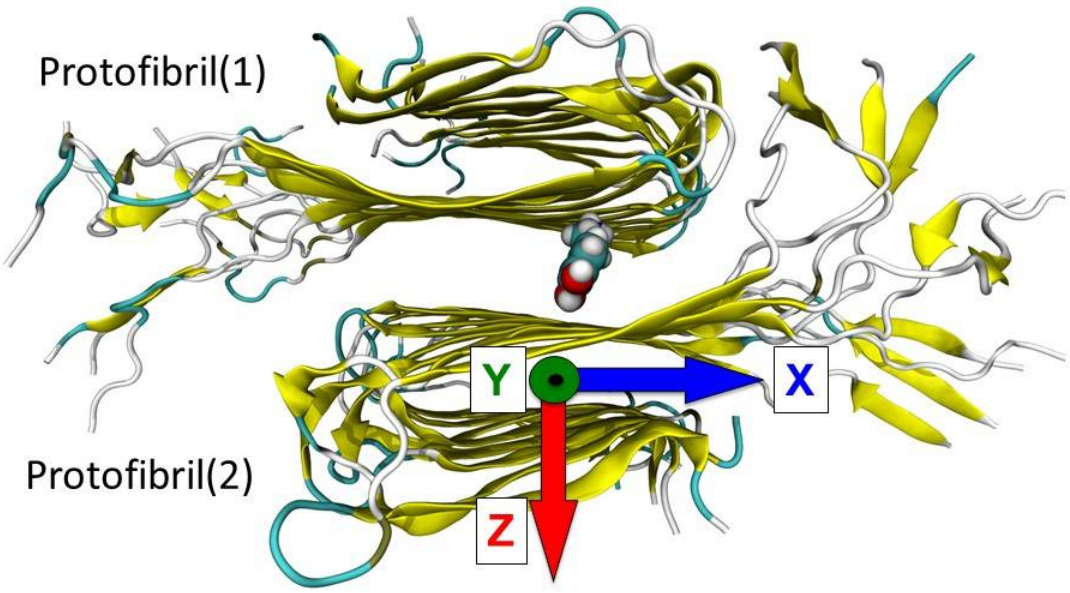

Figure 2: pulling directions applied to protofibril(2) during the calculation of the forces needed for double-layered destruction: *x-axis* (i.e. outward: shift of the protofibril(2) along its secondary axes), the *y-axis* (i.e. lateral, shift of the protofibril(2) along its primary axes) and the *z-axis* (i.e. vertical, progressive removal of protofibril(2)).

3. Results and Discussion

The five natural compounds studied are listed in **Table 1**, together with their effective concentrations (EC_{50}) for the formation, extension and destabilization of preformed Aβ(1-40) (fAβ(1-40)).

The overall *in vitro* activities of **CUR** and **ROSM** are similar [54]. Moreover, *in vivo* observations suggest that curcumin may be beneficial even after the disease has developed, reducing amyloid levels and plaque burden of aged mice with advanced amyloid accumulation[55]. Quercetin (**QUER**) shows moderate *in vitro* preformed fAβ(1-40) destabilization effects with respect to CUR [56]. (-)-epigallocatechin-3-gallate (**EGCG**) is undergoing phase II–III clinical trials as inhibitor of Aβ fibrillogenesis. It decreases plaque burdens in the brain, and reduces soluble and insoluble preformed fAβ(1-40)s [57]. Finally, Dopamine (**DOPA**) proved to be a potent anti-amyloidogenic agent at all the different levels of formation, extension of amyloid fibrils and destabilization of preformed fAβ(1–40)s [58].

Heterogeneity in the experimental conditions (i.e. peptide concentrations, incubation condition and procedure of fAβ preparation) used in different laboratories or different experiments in the same lab gives rise of discrepancy in effective EC_{50} concentrations, thus preventing a quantitative rationalization of the observed experimental trend by means of the results of the computational simulations. However, some interesting qualitative structure-activity relationships could be considered, as shown in the following.

Preprints (www.preprints.org) | NOT PEER-REVIEWED | Posted: 27 May 2018 doi:10.20944/preprints201805.0380.v1

Peer-reviewed version available at Molecules 2018, 23, 1320; doi:10.3390/molecules23061320

Table 1. The effective concentrations (EC_{50}) of the ligands studied for the formation, extension and destabilization of fAβ(1-40).

Compound	Acronym	Structure	Aβ(1-40) formation (EC_{50}) μM	Aβ(1-40) extension (EC_{50}) μM	Aβ(1-40) destabilization (EC_{50}) μM
Curcumin diketo form	CUR-di	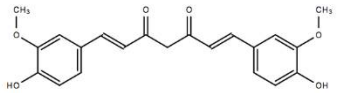	0.19[54] 0.81[55]	0.19[54]	0.42[54] 1.00[55]
Curcumin ketoenol form	CUR-ke	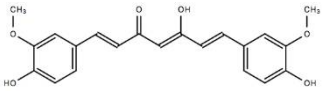			
Dopamine	DOPA	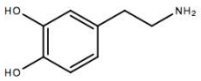	0.01[58]	0.03[58]	0.21[58]
(-)-Epigallocatechin-3-gallate	EGCG	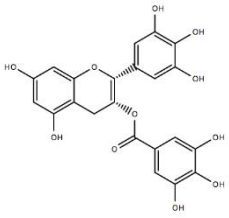	0.18[11]	-	15*[57]
Quercetin	QUER	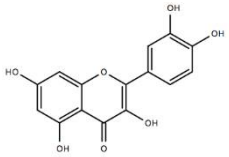	0.24[56]	0.25[56]	2.1[56]
Rosmarinic acid	ROSM	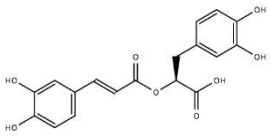	0.29[54]	0.26[54]	0.83[54]

* referred to Aβ(1-42) fibrils.

3.1 Putative Binding sites and Binding Free Energies

Six main binding sites have been highlighted by means of the REMD method applied to the ligands considered. They are located at the surface of the protofibril:

1. **β-1** β-sheet corresponding to the AA sequence ^{16}KLVFFAEDV^{24},
2. **β-2** β-sheet corresponding to the AA sequence ^{31}IIGLMVG^{37},
3. **Elbow** connecting the two β-sheets in correspondence of the AA sequence ^{22}EDVGSN^{27},
4. top of the protofibril **Over** the two β-sheets of the terminal Aβ(1-40) monomer,
5. disordered tails located at the **N-terminal**,
6. end of the β-2 β-sheet, on the **C-terminal** (entry of the cleft).

Preprints (www.preprints.org) | NOT PEER-REVIEWED | Posted: 27 May 2018 doi:10.20944/preprints201805.0380.v1

Peer-reviewed version available at Molecules 2018, 23, 1320; doi:10.3390/molecules23061320

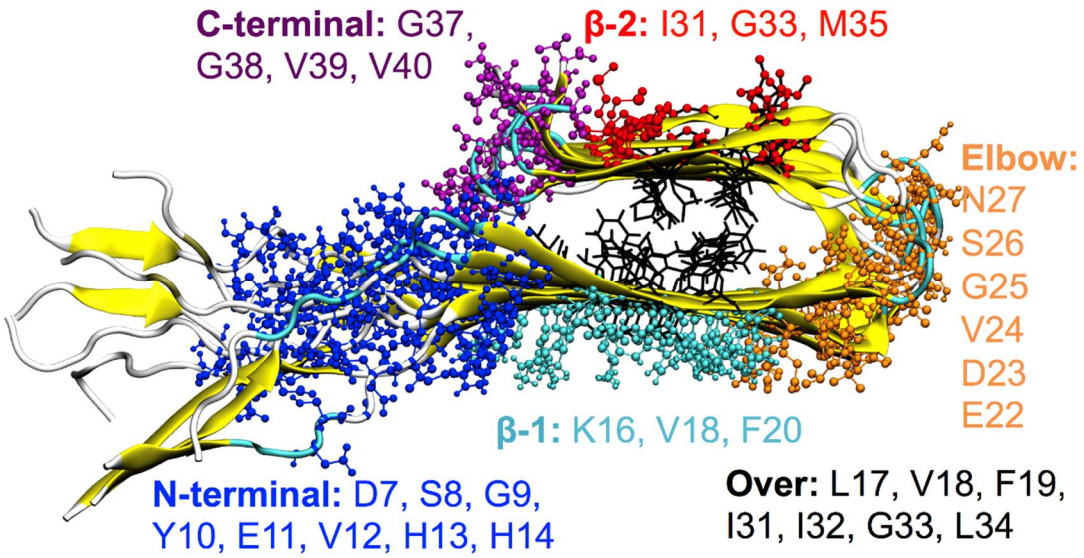

Figure 3: ball-and-stick representation of the ligand binding sites obtained by REMD. Amino-acids (one-letter code) involved in the interactions are reported for each binding site with different colours.

For each binding site, amino acids that make persistent interactions (in this work, an interaction is considered as persistent if the amino acid residue remains in contact with the ligand for at least 60% of the total simulation time) with the ligands and that contributes more than 1 kcal/mol to the binding energy are highlighted in **Figure 3**. The probability of the occupancy of each site is shown in **Figure 4a**.

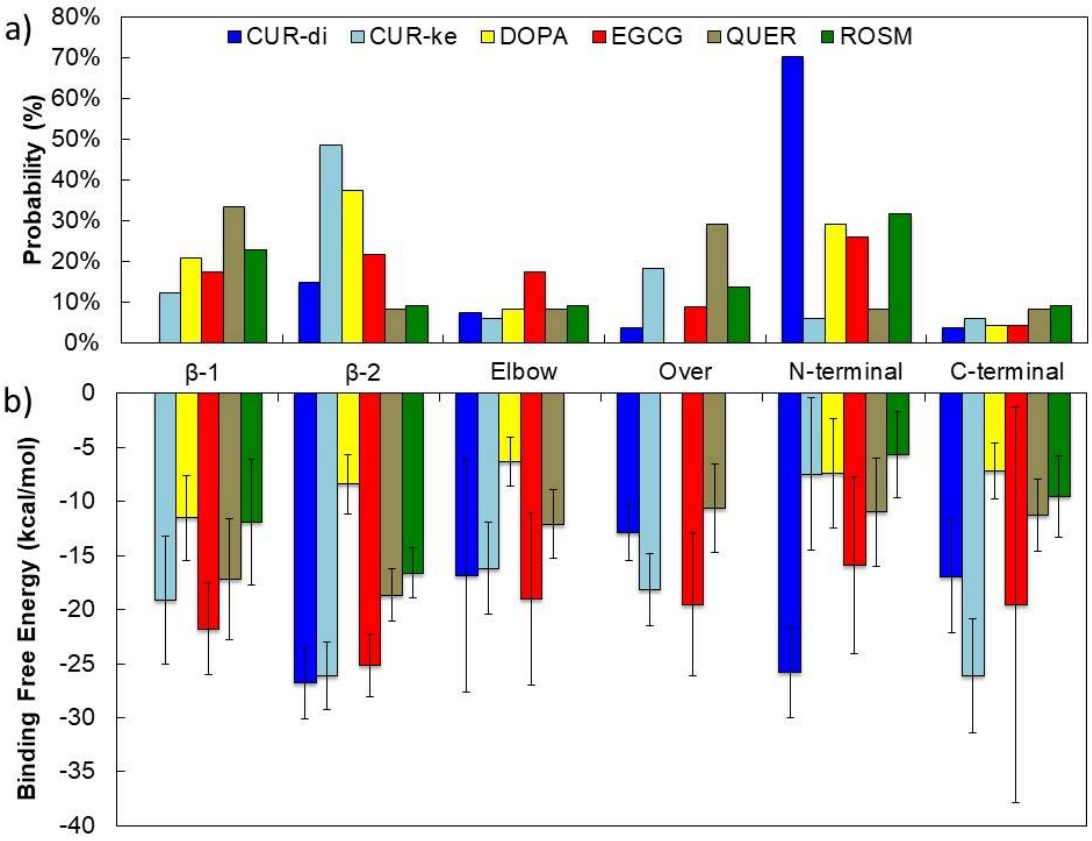

Figure 4: Probability of occupancy of each binding site (a), and binding free energy (b) for each ligand considered

It is interesting to note the different occupancy preferences of the two curcumin's forms. The CUR-di predominantly interacts with the N-terminal, whereas CUR-ke is mainly found at the β-2 site.

Multiple binding sites have been previously described in the literature for curcumin derivatives and others related compounds. In particular, the β-2 site has been very recently targeted in a combined computational and experimental study by Battisti *et al.*[22] aimed at the design of curcumin-like amyloid beta peptides inhibitors. Binding to N-terminal and Over position have been observed for curcumin and other ligands by means of site map analysis by Kundaikar *et al.*[59]. Moreover, the β-1 binding site has previously been suggested as possible binding site for curcumin on the basis of solid-state NMR experiments[60] and computational studies on Aβ hexapeptide ^{16}KLVFFA^{21} and full length Aβ fibrils[19,22].

Although a few studies in the literature proposed the cavity formed by the two β-sheets and the turn as possible binding site for curcumin[24,25] and other compounds such as Orange-G[26] this site is never occupied by the ligands considered in the present study. However, small portions of CUR-ke, EGCG, QUER and ROSM ligands occasionally can penetrate this cavity during the dynamic simulations runs, when they are interacting with the Aβ(1-40) protofibril in the Over position.

By considering the probability of the occupancy of each binding sites (**Figure 4a**) together with the corresponding Binding Free Energies (**Figure 4b**) it emerges that:

- CUR-di and CUR-ke. CUR-ke, the predominant form in aqueous solution on the basis of the recent results obtained by Manolova *et al.*[61], shows a strong propensity to dock at the β-2 site and realizes at this site strong interactions (ΔG_{bind} > -20 kcal/mol) with the fAβ(1-40) fibril. However, moderate to strong (-10 < ΔG_{bind} > -20 kcal/mol) free energies of binding are found for all the binding sites with the exception of the N-terminal one.

-DOPA shows a preference for docking the β-2 and N-ter sites. However, by considering the free energy of binding, it does not show selectivity among the six sites studied, realizing moderate to weak interactions G_{bind} < -10 kcal/mol) with all of them.

- EGCG targets preferentially the N-ter and β-2 sites, and, secondarily, the Elbow and β-1 sites. However, this ligand is able to realize strong binding with all the possible six sites. The most stable complexes (ΔG_{bind} > -20 kcal/mol) are obtained at the β-2, and β-1 sites. The ability of EGCG to bind to the N-terminal amino acids (1-16 residues) is confirmed by results obtained by isothermal titration calorimetry experiments[62]. Moreover, recent findings by solution NMR indicate that EGCG preferentially binds to Aβ oligomers and shield them at the β-1 and β-2 sites,[63] where it remodels the oligomer surface altering the interactions with the monomers.

- QUER is found almost equally distributed between the β-1 and "over" sites with significant lower probability for the other sites. However, it realizes moderate binding free energies (ΔG_{bind} ~ -10 kcal/mol) in all sites, with the most stable complexes (ΔG_{bind} ~ -20 kcal/mol) involving the β-2, and β-1 sites. These results are in agreement with the finding of a computational study recently reported by Ren et al.[20] for a structurally homologous compound, genistein. They showed that genistein prefers to bind the β-sheet grooves to interfere with their self-aggregation.

-ROSM has higher probability for docking at the N-ter and β-1 sites, but realizes the most stable interactions with moderate binding free energies at the β-2 and β-1 sites. Indeed, NMR investigations suggest that a ROSM hairpin-like structure would allow the intercalation into the Aβ oligomers structure, at the interprotofilament (β−β zippers) interface[6].

Thus, taking the error in the computation of the ΔG_{bind} into account, it can be stated that the β-2 grove is a common structural target for all the ligands studied; at this site the ligands realize their most stable interactions with residues M35, G33, and I31. The β-1 site is also targeted for energetically favoured complexes, realized mainly by the interaction with the K16, V18, F20 residues.

These regions are particularly interesting since they constitute the junction between protofilaments in common Aβ(1-40) polymorphs[31,64]. Several recent computational studies employing different multiple protofilament structures and a variety of ligands, used as markers for amyloid detection, indicate the interfacial pockets at the junction between protofilaments as

Preprints (www.preprints.org) | NOT PEER-REVIEWED | Posted: 27 May 2018 doi:10.20944/preprints201805.0380.v1

Peer-reviewed version available at Molecules 2018, 23, 1320; doi:10.3390/molecules23061320

preferential bind sites[26–28]. Binding of ligands at these sites can interfere with the formation or induce the disruption of the aggregates, as discussed in the next section.

In agreement with the previous studies on related compounds [16, 54], the binding free energies obtained for these complexes are driven by more favourable non-polar interactions rather than by electrostatic ones. (Figure S2).

Visual inspection of all MD trajectories shows that the random-coil N-terminal 1DAEFRHDS8 sequence does not alter appreciably the conformation and the usual behaviour of the rest of the fibril, despite its high flexibility promote the nomadism of the ligands that bind preferentially to D7 and S8. Moreover, overall the binding of the ligands do not disturb the structural integrity and secondary structure of the Aβ protofibrils, their overall U-shaped conformations being retained with or without interacting ligands.

However, in a few cases (EGCG, CUR-ke and QUER) when the ligands, during the dynamic run, migrate from the Over site to the β-2 β-sheet in proximity to M35, a perturbation of the fibril secondary structure in the terminal monomers laying at the head of the protofibril is observed. This perturbation, observed in the time of the simulations expecially in the elbow region, induces a bent in the long fibril axis that can impair the process of fibril elongation.

Figure 5 explains the phenomenon for the complex formed by EGCG and the Aβ protofibrils. The side-chain of M35, interacting with the ligand, chaperons it in the search for the best interactions in the β-2 groove, causing a bending of the protofibril and altering the Aβ protofibril secondary structure in the Elbow region. Moreover, the dynamics of the M35 side-chain, induced by the interacting ligand, disrupts the hydrophobic interaction between L34 and F19, which is found to influence a broad range of different processes including the initiation of fibrillation, oligomer stability, fibril elongation, and cellular toxicity[65]. In addition, it is worth undelaying that M35 itself is also known to be responsible for the hierarchical assembly of amyloid fibrils.

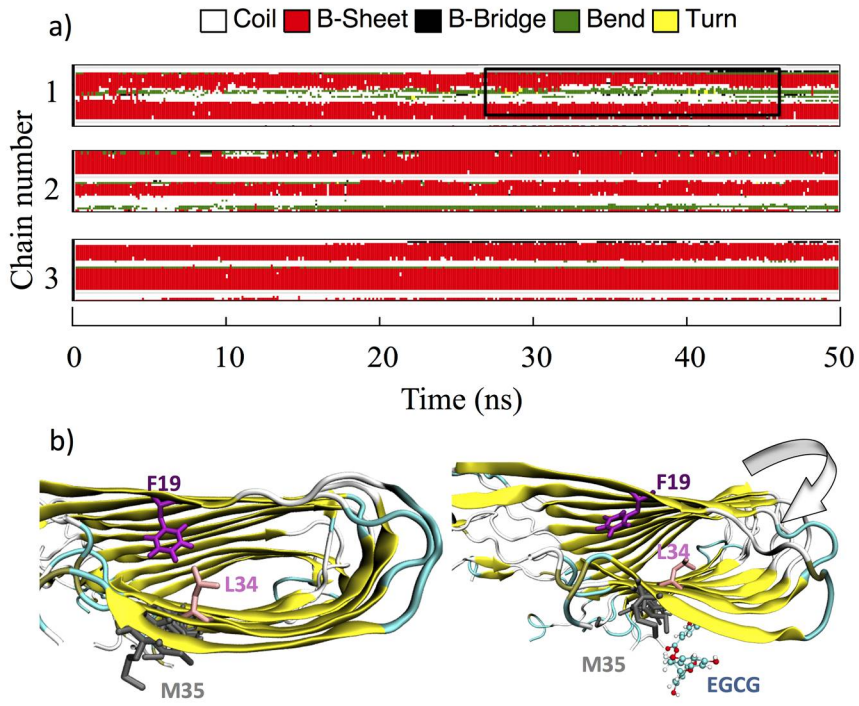

Figure 5: a) Evolution of the Aβ(1-40) secondary structure (computed with the GROMACS DSSP tool) upon EGCG binding on the β-2 β-sheet grove. The perturbation induced at the monomers lying at the head of the protofibril is highlighted by a black box. For clarity safe, only the top three Aβ(1-40) monomers are showed. b) Conformation of F19 and L34 before (left) and after (right) the interaction of EGCG with M35.

3.2 Influence of the ligands on the stability of the Aβ(1-40) oligomer double-layered structures

The effect of the ligands on the stability of the protofibril double-layered structures has been quantified by the calculation of the forces (PMF) for protofibril(1)/ligand-protofibril(2) unbinding. On the basis of the binding site preferences discussed in the previous section, the intercalation of the ligands into the C-terminal–C-terminal and N-terminal–N-terminal interfaces of the protofibrils have been considered. Moreover, three possible ways for complex disruption have been examined by applying the forces along the *x-axis* (i.e. outward: shift of the protofibril(2) along its secondary axes), the *y-axis* (i.e. lateral, shift of the protofibril(2) along its primary axes) and the *z-axis* (i.e. vertical, progressive removal of protofibril(2)), as shown in **Figure 2**.

The results are reported in **Table 2**, together with the force need to separate the pristine protofibril-protofibril aggregation, taken as control.

It is worth noting that the C-terminal–C-terminal interface of the double-layered Aβ-sheets consists of highly hydrophobic patches of I31, I41, and M35, with an average intermolecular distances between the two β-sheets of ~ 9.1 Å (see **Table 3**), whereas the N-terminal–N-terminal interface consists of both hydrophobic patches of V18 and F20 and K16–E22 salt bridges with an average intermolecular distances of ~ 14.3 Å, in agreement with previous computational studies on Aβ17-42 [66] and on different segmental polymorphs (Aβ 35-42, Aβ 16-21, Aβ 27-32) modelled by Berhanu et al.[67]. These characteristics determine the stability of the β-sheet-β-sheet interfaces, which is significantly higher for the N-terminal–N-terminal arrangement with respect to the C-terminal–C-terminal one, as results from the PMF for protofibril(1)-protofibril(2) unbinding, at least for the *vertical* and *outward* directions (**Table 2**).

Table 2: Computed force (expressed in kJ/mol) needed for protofibril(1)-protofibril(2) (control) and protofibril(1)/ligand-protofibril(2) unbinding along the *x, y* and *z-axis*.

Force Direction	***Lateral (x-axis)***		***Vertical (y-axis)***		***Outward (z-axis)***	
Ligand/binding site	β-1	β-2	β-1	β-2	β-1	β-2
Control	2743 ± 115	2772 ± 140	3520 ± 200	2013 ± 30	3413 ± 250	2387 ± 330
CUR-di	2573 ± 40	1913 ± 110	1570 ± 70	1843 ± 35	2810 ± 10	2107 ± 140
CUR-ke	2600 ± 100	2167 ± 280	1653 ± 60	1733 ± 150	2760 ± 70	2633 ± 250
DOPA	2356 ± 95	2180 ± 190	1663 ± 55	1927 ± 420	2150 ± 95	2540 ± 90
EGCG	2968 ± 93	2407 ± 75	1967 ± 25	1610 ± 115	2570 ± 30	2533 ± 60
QUER	2493 ± 90	2043 ± 155	1726 ± 75	1720 ± 30	2553 ± 120	2650 ± 100
ROSM	2888 ± 173	1677 ± 55	2053 ± 40	1367 ± 15	2767 ± 70	2310 ± 105

Overall, the binding of the ligands to β-sheet- β-sheet interfacial pockets located between two protofilaments produces a reduction of the stability of the protofibril dimeric structures. However, this cannot be directly correlated to the increasing in the intermolecular distances between the two interacting protofibril. In fact, for the N-terminal–N-terminal interface, the distance increases upon ligand binding, is in the order of 2 Å, while for the C-terminal–C-terminal one, initially characterized by a tight binding due to hydrophobic interactions, is ~ 4-5 Å. (**Table 3**).

Table 3: Inter-sheet distance in the Aβ(1-40) oligomer double-layered structures

	β-1	**β-2**
Control	14.3 ± 0.3	9.1 ± 0.3
CUR-di	15.7 ± 0.4	13.4 ± 0.3
CUR-ke	15.4 ± 0.3	13.6 ± 0.4
DOPA	16.5 ± 0.5	14.1 ± 0.4
EGCG	16.6 ± 0.5	13.0 ± 0.4
QUER	16.3 ± 0.4	12.7 ± 0.4
ROSM	15.8 ± 0.3	14.1 ± 0.3

On the other hand, the maximum destabilization of the double-layered Aβ-sheet aggregates is observed for the β1-arrangements, when the forces are applied, along the vertical (y) and outward (z), and lateral (x) axes, in the order.

The binding of ligands at the C-terminal–C-terminal interface results in a moderate destabilization of the double-layered Aβ-sheet aggregates with respect to the lateral and vertical modalities, whereas for the outward disruption it appears that the ligands have no effect or operate a small stabilization of the complexes, the large errors obtained do not allow further lucubration.

It is worth noting that the inter-sheet separation produced by DOPA, the smallest ligand, is larger or comparable to the one observed for more cumbersome ligands, and its effect on the destabilization of the protofibril dimeric aggregates is also overall stronger than the other ligands.

4. Concluding remarks

The results of the sistematic computational study carried out on the interaction of five natural biophenols with single Aβ(1-40) protofilament by means of REMD simulations allowed the individuation of multiple binding sites for each ligand located at the surface of the protofibril nearby the β-1 β-sheet, β-2 β-sheet, elbow connecting the two β-sheets, top of the protofibril, disordered N-terminal, and C-terminal.

The REMD methodology used does not allow the biophenols to entry into the hydrophobic core of the preformed protofibril, probably because the energy penalty associate with the penetration process cannot be overcome using conventional MD. The absence of binding sites in the cavity of the preformed protofibril prevent the study of destabilizing effects of the ligands by promotion of disruption of the native backbone hydrogen bonds in the protofibril interior.

The MM_PBSA energetic analysis of the binding shows that the β-1 and β-2 binding sites at the exposed surface of the Aβ(1-40) protofibrils, shared by all the five ligands studied, are thermodynamically favoured. At these sites the anti-amyloid activity of biophenols consists in the inhibition of fibrils thickening and elongation.

In fact, although no significant perturbation of the overall protofibril secondary structure is observed in the periods of time studied, interesting conformational changes of the terminal peptides with subsequent bending of the principal axis of the protofibril is induced by ligands that migrate during the dynamic run from the Over binding site to the β-2 binding site. This effect is more marked for EGCG, but is observed also for CUR-ke and QUER and may preclude the association of an incoming Aβ peptide inhibiting the fibril elongation.

Moreover, ligand binding at the β-2 binding site may inhibit the amyloidogenic process by shielding the M35, which is responsible for the hierarchical assembly of amyloid fibrils, and disrupting the hydrophobic interaction between L34 and F19, which is found to influence a broad range of different processes including the initiation of fibrillation, oligomer stability, fibril elongation, and cellular toxicity.

Finally, the stability of the β-sheet-β-sheet interfaces of the Aβ(1-40) oligomer double-layered structures is significantly affected by the intercalation of the biophenols. The force needed for disruption of the aggregates is halved by all the ligands binding the N-terminal-N-terminal interface, when the forces are applied along the principal axis of the protofibril. The most remarkable effect is observed for DOPA on the double-layered structure in the N-terminal-N-terminal arrangement whatever force direction; whereas ROSM and EGCG exert a stronger destabilization at the double-layered structure in the C-terminal-C-terminal arrangement.

Supplementary Materials: Figure S1.

Author Contributions: Conceptualization, Maria Cristina Menziani; Formal analysis, Francesco Tavanti; Funding acquisition, Maria Cristina Menziani; Investigation, Francesco Tavanti; Methodology, Francesco Tavanti; Project administration, Maria Cristina Menziani; Supervision, Maria Cristina Menziani and Alfonso Pedone; Visualization, Francesco Tavanti; Writing – original draft, Francesco Tavanti; Writing – review & editing, Alfonso Pedone.

Acknowledgments: FT acknowledges the grant FAR2015 from UNIMORE. The authors gratefully acknowledge CINECA supercomputing centre (Italy), HPC projects ISCRA-C HP10CATCHE, for computational resources

References

1. Knowles, T. P. J.; Vendruscolo, M.; Dobson, C. M. The amyloid state and its association with protein misfolding diseases. *Nat. Rev. Mol. Cell Biol.* **2014**, *15*, 384–396, doi:10.1038/nrm3810.
2. Chiti, F.; Dobson, C. M. Protein Misfolding, Functional Amyloid, and Human Disease. *Annu. Rev. Biochem.* **2006**, *75*, 333–366, doi:10.1146/annurev.biochem.75.101304.123901.
3. Eisenberg, D.; Jucker, M. The amyloid state of proteins in human diseases. *Cell* **2012**, *148*, 1188–1203, doi:10.1016/j.cell.2012.02.022.
4. Han, X.; He, G. Toward a Rational Design to Regulate β-Amyloid Fibrillation for Alzheimer's Disease Treatment. *ACS Chem. Neurosci.* **2018**, *9*, 198–210, doi:10.1021/acschemneuro.7b00477.
5. Biophenols pharmacology against the amyloidogenic activity in Alzheimer's disease. *Biomed. Pharmacother.* **2017**, *89*, 396–413, doi:10.1016/j.biopha.2017.02.051.
6. Airoldi, C.; Sironi, E.; Dias, C.; Marcelo, F.; Martins, A.; Rauter, A. P.; Nicotra, F.; Jimenez-Barbero, J. Natural Compounds against Alzheimer's Disease: Molecular Recognition of Aβ1–42 Peptide by Salvia sclareoides Extract and its Major Component, Rosmarinic Acid, as Investigated by NMR. *Chem. – Asian J.* **2013**, *8*, 596–602, doi:10.1002/asia.201201063.
7. Kim, H.; Park, B.-S.; Lee, K.-G.; Choi, C. Y.; Jang, S. S.; Kim, Y.-H.; Lee, S.-E. Effects of Naturally Occurring Compounds on Fibril Formation and Oxidative Stress of β-Amyloid. *J. Agric. Food Chem.* **2005**, *53*, 8537–8541, doi:10.1021/jf051985c.
8. Ngo, S. T.; Li, M. S. Top-leads from natural products for treatment of Alzheimer's disease: docking and molecular dynamics study. *Mol. Simul.* **2013**, *39*, 279–291, doi:10.1080/08927022.2012.718769.
9. Williams, P.; Sorribas, A.; R. Howes, M.-J. Natural products as a source of Alzheimer's drug leads. *Nat. Prod. Rep.* **2011**, *28*, 48–77, doi:10.1039/C0NP00027B.
10. Natural product-based amyloid inhibitors. *Biochem. Pharmacol.* **2017**, *139*, 40–55, doi:10.1016/j.bcp.2017.04.004.
11. Porat Yair; Abramowitz Adel; Gazit Ehud Inhibition of Amyloid Fibril Formation by Polyphenols: Structural Similarity and Aromatic Interactions as a Common Inhibition Mechanism. *Chem. Biol. Drug Des.* **2005**, *67*, 27–37, doi:10.1111/j.1747-0285.2005.00318.x.
12. Lemkul, J. A.; Bevan, D. R. The Role of Molecular Simulations in the Development of Inhibitors of Amyloid β-Peptide Aggregation for the Treatment of Alzheimer's Disease. *ACS Chem. Neurosci.* **2012**, *3*, 845–856, doi:10.1021/cn300091a.
13. Liu, F.-F.; Dong, X.-Y.; He, L.; Middelberg, A. P. J.; Sun, Y. Molecular Insight into Conformational Transition of Amyloid β-Peptide 42 Inhibited by (−)-Epigallocatechin-3-gallate Probed by Molecular Simulations. *J. Phys. Chem. B* **2011**, *115*, 11879–11887, doi:10.1021/jp202640b.
14. Zhao, L. N.; Chiu, S.-W.; Benoit, J.; Chew, L. Y.; Mu, Y. The Effect of Curcumin on the Stability of Aβ Dimers. *J. Phys. Chem. B* **2012**, *116*, 7428–7435, doi:10.1021/jp3034209.
15. Zhang, T.; Zhang, J.; Derreumaux, P.; Mu, Y. Molecular Mechanism of the Inhibition of EGCG on the Alzheimer Aβ1–42 Dimer. *J. Phys. Chem. B* **2013**, *117*, 3993–4002, doi:10.1021/jp312573y.
16. Wang, Y.; Latshaw, D. C.; Hall, C. K. Aggregation of Aβ(17–36) in the Presence of Naturally Occurring Phenolic Inhibitors Using Coarse-Grained Simulations. *J. Mol. Biol.* **2017**, *429*, 3893–3908, doi:10.1016/j.jmb.2017.10.006.
17. Awasthi, M.; Singh, S.; Pandey, V. P.; Dwivedi, U. N. Modulation in the conformational and stability attributes of the Alzheimer's disease associated amyloid-beta mutants and their favorable stabilization by curcumin: molecular dynamics simulation analysis. *J. Biomol. Struct. Dyn.* **2017**, 1–16, doi:10.1080/07391102.2017.1279078.
18. Chebaro, Y.; Jiang, P.; Zang, T.; Mu, Y.; Nguyen, P. H.; Mousseau, N.; Derreumaux, P. Structures of Aβ17–42 Trimers in Isolation and with Five Small-Molecule Drugs Using a Hierarchical Computational Procedure. *J. Phys. Chem. B* **2012**, *116*, 8412–8422, doi:10.1021/jp2118778.
19. Rao, P. P. N.; Mohamed, T.; Teckwani, K.; Tin, G. Curcumin Binding to Beta Amyloid: A Computational Study. *Chem. Biol. Drug Des.* **2015**, *86*, 813–820, doi:10.1111/cbdd.12552.
20. Ren, B.; Liu, Y.; Zhang, Y.; Cai, Y.; Gong, X.; Chang, Y.; Xu, L.; Zheng, J. Genistein: A Dual Inhibitor of Both Amyloid β and Human Islet Amylin Peptides. *ACS Chem. Neurosci.* **2018**, doi:10.1021/acschemneuro.8b00039.
21. Taguchi, R.; Hatayama, K.; Takahashi, T.; Hayashi, T.; Sato, Y.; Sato, D.; Ohta, K.; Nakano, H.; Seki, C.; Endo, Y.; Tokuraku, K.; Uwai, K. Structure–activity relations of rosmarinic acid derivatives for the amyloid

β aggregation inhibition and antioxidant properties. *Eur. J. Med. Chem.* **2017**, *138*, 1066–1075, doi:10.1016/j.ejmech.2017.07.026.

22. Battisti, A.; Piccionello, A. P.; Sgarbossa, A.; Vilasi, S.; Ricci, C.; Ghetti, F.; Spinozzi, F.; Gammazza, A. M.; Giacalone, V.; Martorana, A.; Lauria, A.; Ferrero, C.; Bulone, D.; Rosalia Mangione, M.; Biagio, P. L. S.; Grazia Ortore, M. Curcumin-like compounds designed to modify amyloid beta peptide aggregation patterns. *RSC Adv.* **2017**, *7*, 31714–31724, doi:10.1039/C7RA05300B.
23. Espargaró, A.; Ginex, T.; Vadell, M. del M.; Busquets, M. A.; Estelrich, J.; Muñoz-Torrero, D.; Luque, F. J.; Sabate, R. Combined in Vitro Cell-Based/in Silico Screening of Naturally Occurring Flavonoids and Phenolic Compounds as Potential Anti-Alzheimer Drugs. *J. Nat. Prod.* **2017**, *80*, 278–289, doi:10.1021/acs.jnatprod.6b00643.
24. Ngo, S. T.; Li, M. S. Curcumin Binds to Aβ1–40 Peptides and Fibrils Stronger Than Ibuprofen and Naproxen. *J. Phys. Chem. B* **2012**, *116*, 10165–10175, doi:10.1021/jp302506a.
25. Ngo, S. T.; Fang, S.-T.; Huang, S.-H.; Chou, C.-L.; Huy, P. D. Q.; Li, M. S.; Chen, Y.-C. Anti-arrhythmic Medication Propafenone a Potential Drug for Alzheimer's Disease Inhibiting Aggregation of Aβ: In Silico and in Vitro Studies. *J. Chem. Inf. Model.* **2016**, *56*, 1344–1356, doi:10.1021/acs.jcim.6b00029.
26. Kawai, R.; Araki, M.; Yoshimura, M.; Kamiya, N.; Ono, M.; Saji, H.; Okuno, Y. Core Binding Site of a Thioflavin-T-Derived Imaging Probe on Amyloid β Fibrils Predicted by Computational Methods. *ACS Chem. Neurosci.* **2018**, doi:10.1021/acschemneuro.7b00389.
27. Murugan, N. A.; Halldin, C.; Nordberg, A.; Långström, B.; Ågren, H. The Culprit Is in the Cave: The Core Sites Explain the Binding Profiles of Amyloid-Specific Tracers. *J. Phys. Chem. Lett.* **2016**, *7*, 3313–3321, doi:10.1021/acs.jpclett.6b01586.
28. Peccati, F.; Pantaleone, S.; Riffet, V.; Solans-Monfort, X.; Contreras-García, J.; Guallar, V.; Sodupe, M. Binding of Thioflavin T and Related Probes to Polymorphic Models of Amyloid-β Fibrils. *J. Phys. Chem. B* **2017**, *121*, 8926–8934, doi:10.1021/acs.jpcb.7b06675.
29. Schmid, N.; Eichenberger, A. P.; Choutko, A.; Riniker, S.; Winger, M.; Mark, A. E.; van Gunsteren, W. F. Definition and testing of the GROMOS force-field versions 54A7 and 54B7. *Eur. Biophys. J. EBJ* **2011**, *40*, 843–856, doi:10.1007/s00249-011-0700-9.
30. Berman, H. M.; Westbrook, J.; Feng, Z.; Gilliland, G.; Bhat, T. N.; Weissig, H.; Shindyalov, I. N.; Bourne, P. E. The Protein Data Bank. *Nucleic Acids Res.* **2000**, *28*, 235–242, doi:10.1093/nar/28.1.235.
31. Petkova, A. T.; Yau, W.-M.; Tycko, R. Experimental Constraints on Quaternary Structure in Alzheimer's β-Amyloid Fibrils†. *Biochemistry (Mosc.)* **2006**, *45*, 498–512, doi:10.1021/bi051952q.
32. Humphrey, W.; Dalke, A.; Schulten, K. VMD: visual molecular dynamics. *J. Mol. Graph.* **1996**, *14*, 33–38, 27–28.
33. Drozdetskiy, A.; Cole, C.; Procter, J.; Barton, G. J. JPred4: a protein secondary structure prediction server. *Nucleic Acids Res.* **2015**, *43*, W389–W394, doi:10.1093/nar/gkv332.
34. Eswar, N.; Webb, B.; Marti-Renom, M. A.; Madhusudhan, M. S.; Eramian, D.; Shen, M.-Y.; Pieper, U.; Sali, A. Comparative protein structure modeling using Modeller. *Curr. Protoc. Bioinforma.* **2006**, *Chapter 5*, Unit 5.6, doi:10.1002/0471250953.bi0506s15.
35. Pronk, S.; Páll, S.; Schulz, R.; Larsson, P.; Bjelkmar, P.; Apostolov, R.; Shirts, M. R.; Smith, J. C.; Kasson, P. M.; van der Spoel, D.; Hess, B.; Lindahl, E. GROMACS 4.5: a high-throughput and highly parallel open source molecular simulation toolkit. *Bioinforma. Oxf. Engl.* **2013**, *29*, 845–854, doi:10.1093/bioinformatics/btt055.
36. Koziara, K. B.; Stroet, M.; Malde, A. K.; Mark, A. E. Testing and validation of the Automated Topology Builder (ATB) version 2.0: prediction of hydration free enthalpies. *J. Comput. Aided Mol. Des.* **2014**, *28*, 221–233, doi:10.1007/s10822-014-9713-7.
37. Malde, A. K.; Zuo, L.; Breeze, M.; Stroet, M.; Poger, D.; Nair, P. C.; Oostenbrink, C.; Mark, A. E. An Automated Force Field Topology Builder (ATB) and Repository: Version 1.0. *J. Chem. Theory Comput.* **2011**, *7*, 4026–4037, doi:10.1021/ct200196m.
38. Berendsen, H. J. C.; Postma, J. P. M.; Gunsteren, W. F. van; Hermans, J. Interaction Models for Water in Relation to Protein Hydration. In *Intermolecular Forces*; Pullman, B., Ed.; The Jerusalem Symposia on Quantum Chemistry and Biochemistry; Springer Netherlands, 1981; pp. 331–342 ISBN 978-90-481-8368-5.
39. Darden, T.; York, D.; Pedersen, L. Particle mesh Ewald: An N·log(N) method for Ewald sums in large systems. *J. Chem. Phys.* **1993**, *98*, 10089–10092, doi:10.1063/1.464397.

40. Essmann, U.; Perera, L.; Berkowitz, M. L.; Darden, T.; Lee, H.; Pedersen, L. G. A smooth particle mesh Ewald method. *J. Chem. Phys.* **1995**, *103*, 8577–8593, doi:10.1063/1.470117.
41. Abraham M. J.; van der Spoel D.; Lindahl E.; Hess B.; and the GROMACS development team GROMACS: High performance molecular simulations through multi-level parallelism from laptops to supercomputers. *GROMACS User Man. Version 504*.
42. Patriksson, A.; Spoel, D. van der A temperature predictor for parallel tempering simulations. *Phys. Chem. Chem. Phys.* **2008**, *10*, 2073–2077, doi:10.1039/B716554D.
43. Ngo, S. T.; Hung, H. M.; Tran, K. N.; Nguyen, M. T. Replica exchange molecular dynamics study of the amyloid beta (11–40) trimer penetrating a membrane. *RSC Adv.* **2017**, *7*, 7346–7357, doi:10.1039/C6RA26461A.
44. Kumari, R.; Kumar, R.; Lynn, A. g_mmpbsa—A GROMACS Tool for High-Throughput MM-PBSA Calculations. *J. Chem. Inf. Model.* **2014**, *54*, 1951–1962, doi:10.1021/ci500020m.
45. Shrake, A.; Rupley, J. A. Environment and exposure to solvent of protein atoms. Lysozyme and insulin. *J. Mol. Biol.* **1973**, *79*, 351–371, doi:10.1016/0022-2836(73)90011-9.
46. Sitkoff, D.; Sharp, K. A.; Honig, B. Accurate Calculation of Hydration Free Energies Using Macroscopic Solvent Models. *J. Phys. Chem.* **1994**, *98*, 1978–1988, doi:10.1021/j100058a043.
47. Sharp, K. A.; Honig, B. Electrostatic interactions in macromolecules: theory and applications. *Annu. Rev. Biophys. Biophys. Chem.* **1990**, *19*, 301–332, doi:10.1146/annurev.bb.19.060190.001505.
48. Baker, N. A.; Sept, D.; Joseph, S.; Holst, M. J.; McCammon, J. A. Electrostatics of nanosystems: Application to microtubules and the ribosome. *Proc. Natl. Acad. Sci.* **2001**, *98*, 10037–10041, doi:10.1073/pnas.181342398.
49. Baron, R.; Hünenberger, P. H.; McCammon, J. A. Absolute Single-Molecule Entropies from Quasi-Harmonic Analysis of Microsecond Molecular Dynamics: Correction Terms and Convergence Properties. *J. Chem. Theory Comput.* **2009**, *5*, 3150–3160, doi:10.1021/ct900373z.
50. Tycko, R. Molecular structure of amyloid fibrils: insights from solid-state NMR. *Q. Rev. Biophys.* **2006**, *39*, 1–55, doi:10.1017/S0033583506004173.
51. Tycko, R. Amyloid Polymorphism: Structural Basis and Neurobiological Relevance. *Neuron* **2015**, *86*, 632–645, doi:10.1016/j.neuron.2015.03.017.
52. Trzesniak Daniel; Kunz Anna-Pitschna E.; van Gunsteren Wilfred F. A Comparison of Methods to Compute the Potential of Mean Force. *ChemPhysChem* **2006**, *8*, 162–169, doi:10.1002/cphc.200600527.
53. Roux, B. The calculation of the potential of mean force using computer simulations. *Comput. Phys. Commun.* **1995**, *91*, 275–282, doi:10.1016/0010-4655(95)00053-I.
54. Ono, K.; Hasegawa, K.; Naiki, H.; Yamada, M. Curcumin has potent anti-amyloidogenic effects for Alzheimer's β-amyloid fibrils in vitro. *J. Neurosci. Res.* **2004**, *75*, 742–750, doi:10.1002/jnr.20025.
55. Yang, F.; Lim, G. P.; Begum, A. N.; Ubeda, O. J.; Simmons, M. R.; Ambegaokar, S. S.; Chen, P. P.; Kayed, R.; Glabe, C. G.; Frautschy, S. A.; Cole, G. M. Curcumin Inhibits Formation of Amyloid β Oligomers and Fibrils, Binds Plaques, and Reduces Amyloid in Vivo. *J. Biol. Chem.* **2005**, *280*, 5892–5901, doi:10.1074/jbc.M404751200.
56. Ono, K.; Yoshiike, Y.; Takashima, A.; Hasegawa, K.; Naiki, H.; Yamada, M. Potent anti-amyloidogenic and fibril-destabilizing effects of polyphenols in vitro: implications for the prevention and therapeutics of Alzheimer's disease. *J. Neurochem.* **2003**, *87*, 172–181, doi:10.1046/j.1471-4159.2003.01976.x.
57. Bieschke, J.; Russ, J.; Friedrich, R. P.; Ehrnhoefer, D. E.; Wobst, H.; Neugebauer, K.; Wanker, E. E. EGCG remodels mature α-synuclein and amyloid-β fibrils and reduces cellular toxicity. *Proc. Natl. Acad. Sci.* **2010**, *107*, 7710–7715, doi:10.1073/pnas.0910723107.
58. Ono, K.; Hasegawa, K.; Naiki, H.; Yamada, M. Anti-Parkinsonian agents have anti-amyloidogenic activity for Alzheimer's beta-amyloid fibrils in vitro. *Neurochem. Int.* **2006**, *48*, 275–285, doi:10.1016/j.neuint.2005.11.001.
59. Kundaikar, H. S.; Degani, M. S. Insights into the Interaction Mechanism of Ligands with Aβ42 Based on Molecular Dynamics Simulations and Mechanics: Implications of Role of Common Binding Site in Drug Design for Alzheimer's Disease. *Chem. Biol. Drug Des.* **2015**, *86*, 805–812, doi:10.1111/cbdd.12555.
60. Masuda, Y.; Fukuchi, M.; Yatagawa, T.; Tada, M.; Takeda, K.; Irie, K.; Akagi, K.; Monobe, Y.; Imazawa, T.; Takegoshi, K. Solid-state NMR analysis of interaction sites of curcumin and 42-residue amyloid β-protein fibrils. *Bioorg. Med. Chem.* **2011**, *19*, 5967–5974, doi:10.1016/j.bmc.2011.08.052.

61. Manolova, Y.; Deneva, V.; Antonov, L.; Drakalska, E.; Momekova, D.; Lambov, N. The effect of the water on the curcumin tautomerism: A quantitative approach. *Spectrochim. Acta. A. Mol. Biomol. Spectrosc.* **2014**, *132*, 815–820, doi:10.1016/j.saa.2014.05.096.
62. Wang, S.-H.; Dong, X.-Y.; Sun, Y. Thermodynamic Analysis of the Molecular Interactions between Amyloid β-Protein Fragments and (−)-Epigallocatechin-3-gallate. *J. Phys. Chem. B* **2012**, *116*, 5803–5809, doi:10.1021/jp209406t.
63. Ahmed, R.; Melacini, G. A solution NMR toolset to probe the molecular mechanisms of amyloid inhibitors. *Chem. Commun.* **2018**, doi:10.1039/C8CC01380B.
64. Bertini, I.; Gonnelli, L.; Luchinat, C.; Mao, J.; Nesi, A. A New Structural Model of Aβ40 Fibrils. *J. Am. Chem. Soc.* **2011**, *133*, 16013–16022, doi:10.1021/ja2035859.
65. Korn, A.; McLennan, S.; Adler, J.; Krueger, M.; Surendran, D.; Maiti, S.; Huster, D. Amyloid β (1-40) Toxicity Depends on the Molecular Contact between Phenylalanine 19 and Leucine 34. *ACS Chem. Neurosci.* **2017**, doi:10.1021/acschemneuro.7b00360.
66. Zheng, J.; Jang, H.; Ma, B.; Tsai, C.-J.; Nussinov, R. Modeling the Alzheimer Aβ17-42 Fibril Architecture: Tight Intermolecular Sheet-Sheet Association and Intramolecular Hydrated Cavities. *Biophys. J.* **2007**, *93*, 3046–3057, doi:10.1529/biophysj.107.110700.
67. Berhanu, W. M.; Hansmann, U. H. E. Structure and Dynamics of Amyloid-β Segmental Polymorphisms. *PLOS ONE* **2012**, *7*, e41479, doi:10.1371/journal.pone.0041479.
68. Re, F.; Airoldi, C.; Zona, C.; Masserini, M.; Ferla, B. L.; Nicotra, N. Q. and F. Beta Amyloid Aggregation Inhibitors: Small Molecules as Candidate Drugs for Therapy of Alzheimers Disease Available online: http://www.eurekaselect.com/72179/article (accessed on Dec 18, 2017).
69. Landau, M.; Sawaya, M. R.; Faull, K. F.; Laganowsky, A.; Jiang, L.; Sievers, S. A.; Liu, J.; Barrio, J. R.; Eisenberg, D. Towards a Pharmacophore for Amyloid. *PLoS Biol* **2011**, *9*, e1001080, doi:10.1371/journal.pbio.1001080.
70. Sievers, S. A.; Karanicolas, J.; Chang, H. W.; Zhao, A.; Jiang, L.; Zirafi, O.; Stevens, J. T.; Münch, J.; Baker, D.; Eisenberg, D. Structure-based design of non-natural amino-acid inhibitors of amyloid fibril formation. *Nature* **2011**, *475*, 96–100, doi:10.1038/nature10154.
71. Jiang, L.; Liu, C.; Leibly, D.; Landau, M.; Zhao, M.; Hughes, M. P.; Eisenberg, D. S. Structure-based discovery of fiber-binding compounds that reduce the cytotoxicity of amyloid beta. *eLife* **2013**, *2*, e00857, doi:10.7554/eLife.00857.
72. Zheng, J.; Baghkhanian, A. M.; Nowick, J. S. A Hydrophobic Surface Is Essential To Inhibit the Aggregation of a Tau-Protein-Derived Hexapeptide. *J. Am. Chem. Soc.* **2013**, *135*, 6846–6852, doi:10.1021/ja310817d.
73. Matthes, D.; Gapsys, V.; Brennecke, J. T.; Groot, B. L. de An Atomistic View of Amyloidogenic Self-assembly: Structure and Dynamics of Heterogeneous Conformational States in the Pre-nucleation Phase. *Sci. Rep.* **2016**, *6*, 33156, doi:10.1038/srep33156.